Aalborg Universitet

AALBORG UNIVERSITY

Simplified Thermal Modeling for IGBT Modules with Periodic Power Loss Profiles in Modular Multilevel Converters

Zhang, Yi; Wang, Huai; Wang, Zhongxu; Yang, Yongheng; Blaabjerg, Frede

Simplified Thermal Modeling for IGBT Modules with Periodic Power Loss Profiles in Modular Multilevel Converters

Yi Zhang, *Student Member, IEEE*, Huai Wang, *Senior Member, IEEE*, Zhongxu Wang, *Student Member, IEEE*, Yongheng Yang, *Senior Member, IEEE*, and Frede Blaabjerg, *Fellow, IEEE*

Abstract—One of the future challenges in Modular Multilevel Converters (MMCs) is how to size key components with compromised costs and design margins, while fulfilling specific reliability targets. It demands better thermal modeling compared to the state-of-the-arts in terms of both accuracy and simplicity. Different from two-level power converters, MMCs have inherent dc-bias in arm currents and the power device conduction time is affected by operational parameters. A time-wise thermal modeling for the power devices in MMCs is therefore an iteration process and time-consuming. This paper thus proposes a simply analytical thermal modeling method, which adopts equivalent periodic power loss profiles. More importantly, time-domain simulations are not required in the proposed method. Benchmarking of the proposed methods with the prior-art solutions is performed in terms of parameter sensitivity and model accuracy with a case study on a 30-MW MMC system. Experiments are carried out on a specifically designed scaled-down system to verify the electro-thermal aspects.

Index Terms—Insulated gate bipolar transistor (IGBT), modular multilevel converter (MMC), power semiconductor, reliability, thermal stress estimation, thermal design.

I. INTRODUCTION

MODULAR Multilevel Converters (MMCs) are promising in medium- and high-power applications [1]. In High-Voltage Direct Current (HVDC) transmissions [2], [3] and high-power motor drive systems [4], MMC systems rated of more than 1000 MW are commissioned or planned [5].

In the literature, many research efforts have been devoted to the basic operation and control of MMCs, such as capacitor voltage balancing [6], steady-state modeling [7], modulation [8], and circulating current control [9]. However, as the MMC is the key equipment in HVDC systems, which are exposed to harsh environments, the reliability has become a major concern. Unfortunately, most of the prior-art reliability studies of the MMC focused on the post-failure protection (e.g., redundancy [10] and fault protection [11]). Design for Reliability (DfR) [12] was introduced to power electronic systems to fulfill the reliability target in the design process. However, the

DfR concept is rarely considered in MMC systems. To reach the reliability target with DfR, a component-level reliability analysis should be performed first. As a great deal of IGBT power devices are used in MMCs, the reliability of the IGBT power devices is then critical, as a prerequisite for the lifetime prediction of the entire system [13].

In respect to the reliability analysis of the IGBT modules, junction temperature swings contribute to repetitive thermal-mechanical stresses, which in return are accumulated as fatigue on the devices. Consequently, the estimation of the thermal behaviors (i.e., temperature swings) is essential for the lifetime prediction and also for the DfR. In [14], temperature swings are classified into two categories: 1) thermal cycling due to load variations with mission profiles, typically varying from seconds to minutes, and 2) thermal stresses at the periodic power loss profiles due to fundamental-frequency currents. Compared with the first type of temperature swings, the amplitude of the thermal cycling at the periodic power loss profile is relatively small in typical applications. However, the accumulated fatigue cannot be ignored, as pointed out in [14] and [15]. Moreover, it has been experimentally verified in [16] that a large number of minor thermal cycles actually accelerate the aging of the power devices towards the end of life. Nevertheless, the impact of the thermal stresses at the periodic power loss profiles is commonly neglected in the lifetime prediction of MMCs [17], leading to inaccuracy. To improve the reliability prediction, the thermal behaviors at the periodic power loss profile should be considered and properly estimated.

Moreover, in respect to the design of cooling systems, a proper estimation of the junction temperature swings is also important. This is more critical in MMC-based motor drive applications [4]. In this case, the minimum fundamental frequency at the rated power can be as small as 2 to 5 Hz. According to [18], for a typical IGBT module, the maximum junction temperature swings in such applications may exceed up to 3 or more times than the value at 50 Hz. Hence, it further emphasizes the estimation of thermal swings at the periodic power loss profiles.

However, there are many challenging issues to be tackled when estimating the thermal stresses. In two-level conventional converters, the IGBT chips and the diodes of an IGBT module are conducting in a half of the cycle period. This means that the power losses in the devices appear only for one half-period.
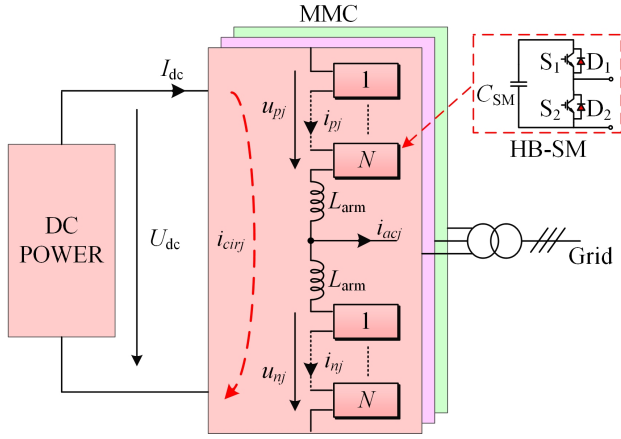
Fig. 1. Configuration of a Modular Multilevel Converter (MMC) system, where U_{dc} is the dc-link voltage, I_{dc} is the dc input current, $u_{p(n)j}$ are arm voltages (p = upper arm, n = lower arm, $j = a, b, c$), $i_{p(n)j}$ are arm currents, i_{cirj} is the circulating current, i_{acj} is the current of the phase j, L_{arm} is the arm inductor, C_{SM} is the sub-module (SM) capacitor, N is the number of SM per arm and HB-SM denotes a half-bridge SM.

Then, the junction temperature varying within the period of the fundamental frequency can be obtained, considering a fixed half sine loss profile [19] or a fixed square loss profile [18]. However, since the inherent dc-bias exists in the arm currents of the MMC, the IGBT chips and the diodes are not conducting 50 % in a cycle of the fundamental frequency. The loss duration for power devices of the MMC is tightly coupled with its operational parameters, which leads to more complicated calculation of the junction temperature behaviors at periodic power loss profiles.

Therefore, this paper proposes a simply thermal modeling method to estimate junction temperature swings at periodic power loss profiles for the power devices in MMC systems. The impact of operational parameters are also considered. The rest of this paper is organized as follows: in Section II, the configuration of an MMC system and the instantaneous power device losses are discussed. Following, an equivalent loss curve is proposed to estimate the junction temperature behaviors. Considering the operational parameters, the equivalent loss curve has the same energy and the same loss duration as the instantaneous power loss profile. Thermal equations are then used to map the junction temperature swings. In Section IV, the parameter sensitivity is discussed with simulations on a full-scale 30-MW MMC system. Additionally, experimental tests on a down-scale system are provided in Section V. Both simulation and experimental results validate the analysis. Finally, concluding remarks are provided in Section VI.

II. SYSTEM DESCRIPTION AND INSTANTANEOUS POWER LOSSES

A. Circuit Configuration of an MMC

Fig. 1 shows the schematic diagram of a typical three-phase MMC system. Each phase of the MMC consists of two arms and each arm comprises N sub-modules (SMs) connected in series and an arm inductor L_{arm}. In each SM, half-bridge (HB) and full-bridge topologies can be adopted [2], [5], [20], where

the most commonly adopted topology is the HB-SM as shown in Fig. 1. Clearly, there are two IGBT modules, that is, the upper IGBT module (denoted as S_1 and D_1) and the lower IGBT module (S_2 and D_2).

The following analysis is valid for any of the six arms of the MMC. For simplicity, the subscripts of a, b, c have been omitted. In steady-state, the arm current consists of a sinusoidal component at the fundamental frequency, a dc-bias depending on the active power, and additional even-order harmonics (i.e., 2nd, 4th, 6th, ...). However, as a circulating current control scheme can be embedded in MMC systems, the even-order harmonics are relatively small and have negligible effects on the electro-thermal behaviors. Then, the arm currents can be written as

$$\begin{cases} i_p = \dfrac{1}{3}I_{\mathrm{dc}} + \dfrac{1}{2}I_{\mathrm{ac}}\sin\left(\omega t - \varphi\right) \\ i_n = \dfrac{1}{3}I_{\mathrm{dc}} - \dfrac{1}{2}I_{\mathrm{ac}}\sin\left(\omega t - \varphi\right) \end{cases} \tag{1}$$

where I_{ac} is the peak value of the ac current, ω is the angular frequency and φ is the phase-shift angle that denotes the power factor of an MMC system.

With the relationship between the dc current and ac current in [7], the arm currents can be rewritten as

$$\begin{cases} i_p = \dfrac{I_{\mathrm{dc}}}{3}\left[1 + \dfrac{2}{m\cos\varphi}\sin\left(\omega t - \varphi\right)\right] \\ i_n = \dfrac{I_{\mathrm{dc}}}{3}\left[1 - \dfrac{2}{m\cos\varphi}\sin\left(\omega t - \varphi\right)\right] \end{cases} \tag{2}$$

in which m is the modulation index ($m = 2U_{\mathrm{ac}}/U_{\mathrm{dc}}$) and U_{ac} is the maximum value of the ac voltage.

According to [7], the insertion indexes of the upper arm and the lower arm are denoted by N_p and N_n, that is

$$\begin{cases} N_p = \dfrac{1}{2}\left(1 - m\sin\left(\omega t\right)\right) \\ N_n = \dfrac{1}{2}\left(1 + m\sin\left(\omega t\right)\right). \end{cases} \tag{3}$$

Taking an SM in the upper arm as an example, the switching function of S_1 and D_1 is identical with the insertion index of N_p. On the contrary, S_2 and D_2 operate in a complementary way. Therefore, the duty ratios of the four power devices are expressed as

$$\begin{cases} M_{\mathrm{S1}} = \dfrac{1}{2}\left(1 - m\sin\left(\omega t\right)\right), & \text{for } i_p < 0, \\ M_{\mathrm{D1}} = \dfrac{1}{2}\left(1 - m\sin\left(\omega t\right)\right), & \text{for } i_p \geqslant 0, \\ M_{\mathrm{S2}} = \dfrac{1}{2}\left(1 + m\sin\left(\omega t\right)\right), & \text{for } i_p > 0, \\ M_{\mathrm{D2}} = \dfrac{1}{2}\left(1 + m\sin\left(\omega t\right)\right), & \text{for } i_p \leqslant 0, \end{cases} \tag{4}$$

with M_{S1}, M_{D1}, M_{S2} and M_{D2} being the corresponding duty ratio of the devices S_1, D_1, S_2 and D_2.

B. Power Device Loss Distribution

As discussed in [21], the power dissipation of a power device includes conduction losses and switching losses. The average conduction loss $P_{\mathrm{cond\_ave}}$ of a power device is

$$P_{\mathrm{cond\_ave}} = f_0 \cdot \int_0^{1/f_0} p_{\mathrm{cond\_inst}}\left(t\right) dt \tag{5}$$

where the instantaneous conduction loss is

$$p_{\text{cond\_inst}}(t) = u_{\text{cond}}(i_x(t), T_j) \cdot i_x(t) \cdot M(m, t) \quad (6)$$

in which u_{cond} is the conducting voltage, i_x is the conducting current through the power device, and the duty ratio $M(m, t)$ is a function of the modulation index m. In the upper arm of the MMC, i_x is the upper arm current i_p, and the duty ratios are expressed in (4). Furthermore, the conduction voltage $u_{\text{cond}}(i_x(t), T_j)$ of the power devices has a linearized characteristic as

$$u_{\text{cond}}(i_x(t), T_j) = [U_{\text{cond0@}T_{\text{ref}}} + K_{\text{T1}} \cdot (T_j - T_{\text{ref}})] + i_x(t) \cdot [r_{\text{cond0@}T_{\text{ref}}} + K_{\text{T2}} \cdot (T_j - T_{\text{ref}})] \quad (7)$$

with $U_{\text{cond0@}T_{\text{ref}}}$, $r_{\text{cond0@}T_{\text{ref}}}$, K_{T1}, and K_{T2} being the coefficients obtained from the data-sheet. In addition, T_{ref} is the reference temperature, typically at 25°C or 125°C.

Similarly, the average switching loss $P_{\text{sw\_ave}}$ is

$$P_{\text{sw\_ave}} = f_0 \cdot \int_0^{1/f_0} p_{\text{sw\_inst}}(t)\, dt \quad (8)$$

where the instantaneous switching loss is

$$p_{\text{sw\_inst}}(t) = f_{\text{sw}} \cdot E_{\text{sw}}(i_x(t), T_j) \cdot \left(\frac{U_{\text{SM}}}{U_{\text{ref}}}\right)^{K_v} \quad (9)$$

with f_{sw} being the equivalent switching frequency, U_{SM} is the average capacitor voltage of an SM, K_v being the voltage coefficient and U_{ref} being the reference blocking voltage in the data-sheet. The switching energy loss E_{sw} provided in the data-sheet represents the typical energy loss per pulse as

$$E_{\text{sw}}(i_x(t), T_j) = E_{\text{sw}}(i_x(t)) \cdot [1 + K_{\text{T3}} \cdot (T_j - T_{\text{ref}})]. \quad (10)$$

Based on the above analysis, the instantaneous power losses and the average power losses of IGBTs and diodes in an SM are shown in Fig. 2. The instantaneous losses of different power devices have a similar shape as sinusoidal-like half waves, but the loss duration varies. S_1 and D_2 have the same loss duration, and S_2 and D_1 share the same loss duration, as shown in Fig. 2. These characteristics reveal that the losses are inherently unevenly distributed between the power devices in an SM. The loss duration of the power devices is not fixed at 50 % of the fundamental-frequency cycle, which is different from the conventional two-level converters. Therefore, the conventional thermal-behavior estimation methods cannot be directly applied to MMCs.

III. PROPOSED THERMAL ESTIMATION METHOD AT FUNDAMENTAL FREQUENCY

As discussed above, the instantaneous power losses have irregular shapes as well as different loss durations. It is difficult to directly translate the instantaneous power losses into the thermal loading. Therefore, an equivalent loss curve is proposed to replace the instantaneous power loss profile for thermal estimation. The equivalent loss curve should meet two conditions: 1) the same loss duration, and 2) the same energy compared with the instantaneous power loss. This will be described in the following sections.
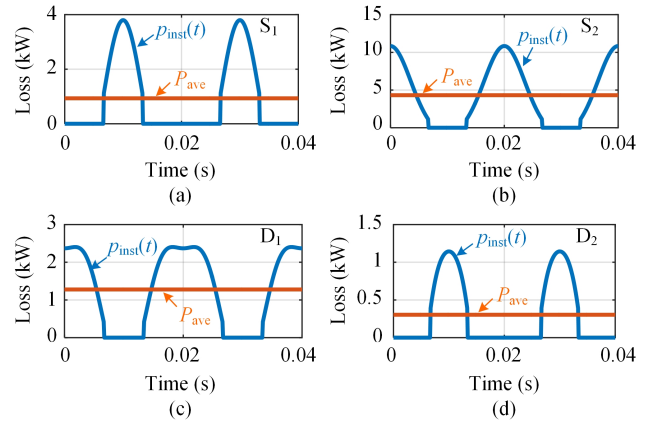

Fig. 2. Instantaneous power losses $p_{\text{inst}}(t)$ and average power losses P_{ave} of IGBTs and diodes in an SM of the 30-MW MMC case: (a) S_1, (b) S_2, (c) D_1, and (d) D_2.
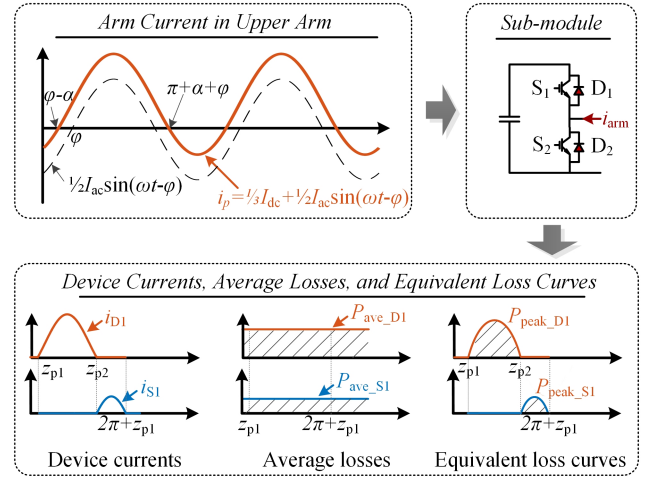

Fig. 3. Equivalent loss curves for the two devices in an upper-arm SM, where the zero points z_{p1} and z_{p2} of the arm current determine the frequencies of the equivalent loss curves.

A. Proposed Equivalent Loss Curve

Firstly, in order to simplify the instantaneous power loss, an equivalent power loss curve is proposed to replace it, which is a sinusoidal half wave as

$$p_{\text{equi\_inst}} = \begin{cases} P_{\text{peak}} \sin(2\pi f_e t), & p_{\text{equi\_inst}} > 0 \\ 0, & p_{\text{equi\_inst}} \leqslant 0 \end{cases} \quad (11)$$

where P_{peak} is the amplitude to describe the average loss, and f_e is the equivalent frequency to characterize the impact of loss profile duration. Then, the key task is to calculate these parameters. As shown in Fig. 3, the locations of the zero points determine the equivalent frequency. According to (2), the zero points of the arm currents can be expressed as

$$\begin{cases} z_{p1} = \varphi - \alpha \\ z_{p2} = \pi + \varphi + \alpha \end{cases}, \text{ with } \alpha = \arcsin\left(\frac{m\cos\varphi}{2}\right) \quad (12)$$

in which z_{p1} and z_{p2} are the two zero points of the upper arm currents. It is obvious that the position of the zero points

TABLE I
EQUIVALENT LOSS CURVES FOR THE DEVICES IN MMCS

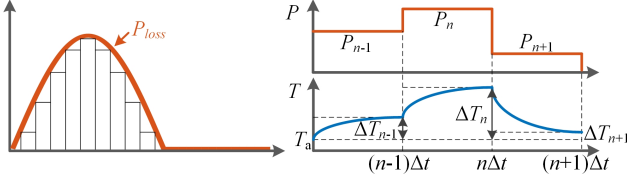| Arm currents		Devices	Conduction period	Loss duration	f_e	P_{peak} of the average power loss
i_p	>0	S_2, D_1	$\varphi - \alpha \leqslant \omega t \leqslant \pi + \varphi + \alpha$	$\pi + 2\alpha$	$\frac{\pi}{\pi+2\alpha} f_0$	$\frac{2\pi^2}{(\pi+2\alpha)[1+\cos(2\alpha)]} P_{\text{ave}}$
	$\leqslant 0$	S_1, D_2	$\pi + \varphi + \alpha \leqslant \omega t \leqslant 2\pi + \varphi - \alpha$	$\pi - 2\alpha$	$\frac{\pi}{\pi-2\alpha} f_0$	$\frac{2\pi^2}{(\pi-2\alpha)[1+\cos(2\alpha)]} P_{\text{ave}}$
i_n	>0	S_2, D_1	$\pi + \varphi - \alpha \leqslant \omega t \leqslant 2\pi + \varphi + \alpha$	$\pi + 2\alpha$	$\frac{\pi}{\pi+2\alpha} f_0$	$\frac{2\pi^2}{(\pi+2\alpha)[1+\cos(2\alpha)]} P_{\text{ave}}$
	$\leqslant 0$	S_1, D_2	$\varphi + \alpha \leqslant \omega t \leqslant \pi + \varphi - \alpha$	$\pi - 2\alpha$	$\frac{\pi}{\pi-2\alpha} f_0$	$\frac{2\pi^2}{(\pi-2\alpha)[1+\cos(2\alpha)]} P_{\text{ave}}$

Fig. 4. Conversion from the equivalent loss curve into the temperature profile at the periodic power loss profile (i.e., at the fundamental frequency).

depends on the phase-shift angle φ and the modulation index m. Furthermore, the equivalent frequencies are obtained as

$$\begin{cases} f_{e1} = \dfrac{\pi}{\pi + 2\alpha} f_0, & \text{for } D_1, \\ f_{e2} = \dfrac{\pi}{\pi - 2\alpha} f_0, & \text{for } S_1. \end{cases} \quad (13)$$

Moreover, the same energy is achieved by an integral calculation. Taking the devices D_1 and S_1 in Fig. 3 as an example, the relationship between the amplitude P_{peak} and the average P_{ave} is expressed as

$$\begin{cases} P_{\text{peak\_D1}} = \dfrac{2\pi^2}{(\pi + 2\alpha)(1 + \cos 2\alpha)} P_{\text{ave}} \\ P_{\text{peak\_S1}} = \dfrac{2\pi^2}{(\pi - 2\alpha)(1 + \cos 2\alpha)} P_{\text{ave}} \end{cases} \quad (14)$$

Therefore, the parameters of (11) are obtained from (13) and (14). Similarly, the equivalent loss curves of S_2, D_2, and the devices in the lower-arm SM are obtained, which is summarized in Table I. It can be observed that the equivalent loss curves are different in the SM but the same between the upper and lower arms, which reveals the thermal unbalance in the SM.

B. Thermal Behaviors Estimation

Based on the equivalent loss curve, an analytical model which enables the estimation of the junction temperature behaviors at periodic power loss profiles is further developed. The equivalent loss curve is divided into n steps, as shown in Fig. 4, where the temperature of one power step is determined by the previous temperature state and the present dissipated power as described in [22]. Then, the thermal model based on a third-order Foster network is obtained as

$$\begin{cases} \Delta T_{n-1} = P_{n-1} \displaystyle\sum_{v=1}^{3} R_{\text{thv}} \left(1 - e^{-\frac{\Delta t}{\tau_{\text{thv}}}}\right) \\ \Delta T_n = \displaystyle\sum_{v=1}^{3} \Delta T_{n-1,v} e^{-\frac{\Delta t}{\tau_{\text{thv}}}} + P_n \sum_{v=1}^{3} R_{\text{thv}} \left(1 - e^{-\frac{\Delta t}{\tau_{\text{thv}}}}\right) \end{cases} \quad (15)$$
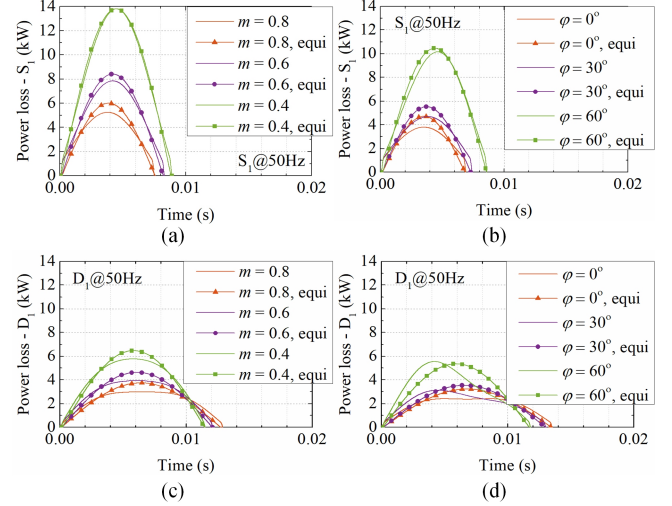

Fig. 5. Instantaneous power losses and the equivalent loss curves of S_1 and D_1 (smooth curves – instantaneous losses, dotted curve (labeled "equi") – proposed equivalent loss curves): (a) power losses of S_1 under different m, (b) under different φ; (c) power losses of D_1 with various m, and (d) with various φ ($\varphi = 0°$ for (a) and (c), $m = 1$ for (b) and (d)).

TABLE II
SPECIFICATIONS OF A FULL-SCALE MMC SYSTEM.

Parameters	Values
System rated active power	P = 30 MW
Rated DC-link voltage	U_{dc} = 31.8 kV
Rated AC grid voltage	U_{ac} = 14 kV
Number of sub-modules per arm	N = 12
Arm inductor	L_{arm} = 4 mH
Arm resistor	R_{arm} = 0.0628 Ω
Sub-module capacitor	C_{SM} = 0.8 mF
Switching frequency	f_{sw} = 1 kHz

where the thermal resistance R_{thv} and time constant τ_{thv} can be found in the data-sheet.

IV. PARAMETER SENSITIVITY ANALYSIS

As presented in (12) to (14), P_{peak} and f_e of the equivalent loss curve are dependent on the modulation index m and the phase-shift angle φ. Thus, a parameter sensitivity analysis is necessary. A full-scale MMC is built up on the MATLAB and PLECS co-simulation platform to analyze the parameter sensitivity, and the specifications are listed in Table II. Moreover, as presented in [23], for the power modules, the rating of 4.5 kV and 1.2 kA is the most commonly adopted for MMC systems.
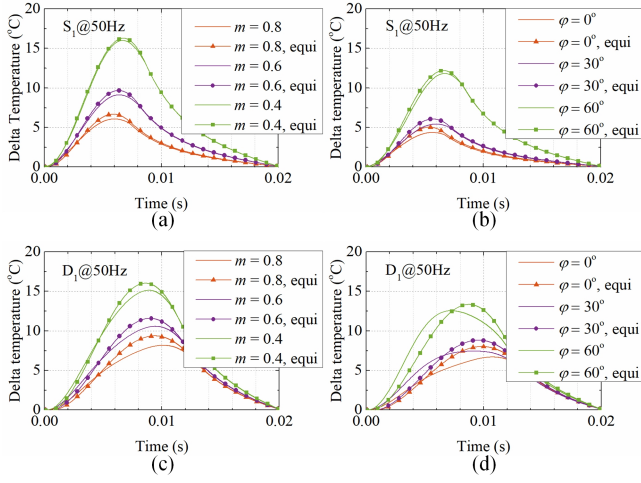
Fig. 6. Thermal profiles based on the instantaneous losses and the equivalent loss curves in S_1 and D_1 at 50 Hz: (a) thermal profiles of S_1 under different m, (b) under different φ; (c) thermal profiles of D_1 with various m, and (d) with various φ ($\varphi = 0°$ for (a) and (c), $m = 1$ for (b) and (d)).

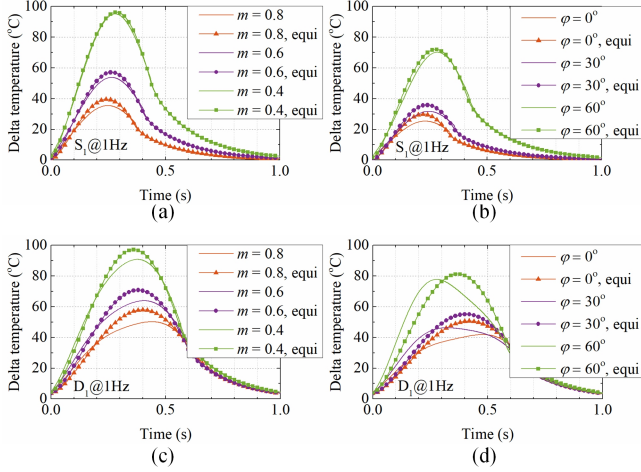Fig. 8. Thermal profiles (simulation results) of the four power devices in the full-scale MMC.

Fig. 7. Thermal profiles based on the instantaneous losses and the equivalent loss curves in S_1 and D_1 at 1 Hz: (a) thermal profiles of S_1 under different m, (b) under different φ; (c) thermal profiles of D_1 with various m, (d) with various φ ($\varphi = 0°$ for (a) and (c), $m = 1$ for (b) and (d)).

Fig. 9. Thermal profiles (calculated results) of the four power devices with the same condition in the simulation: (a) absolute temperatures and (b) temperature variations.

Therefore, IGBT modules from ABB 5SNA1200G450350 (4.5 kV/1.2 kA) are chosen as the power module for the HB-SM in the full-scale MMC system in simulations.

A. Sensitivity of the Proposed Model

A comparison between the instantaneous losses and the equivalent loss curves of S_1 and D_1 is illustrated in Fig. 5. Three equivalent loss curves have the same loss duration with the corresponding instantaneous losses as well as the similar shapes. Moreover, due to the inherent dc-bias in the arm currents, the loss duration of S_1 is always smaller than 0.01 s (half period of 50 Hz), while the loss duration of D_1 is over 0.01 s in all cases. As shown in Figs. 5(a) and (b), the peak losses of S_1 increase with a smaller modulation index m or a larger phase-shifted angle φ, since the average losses
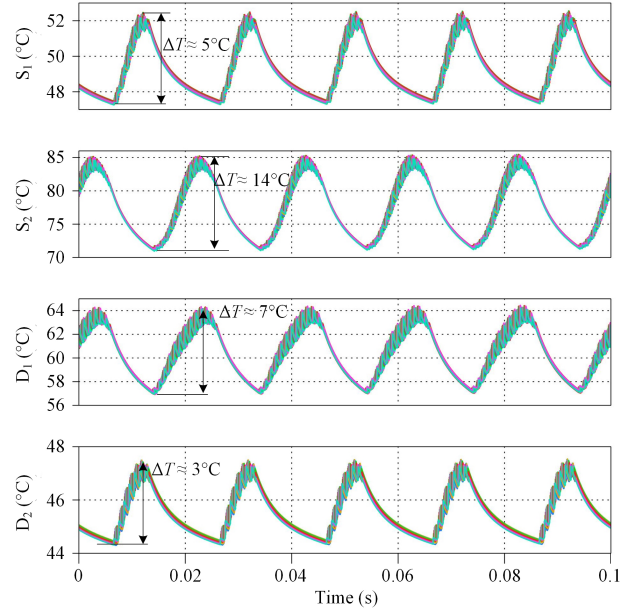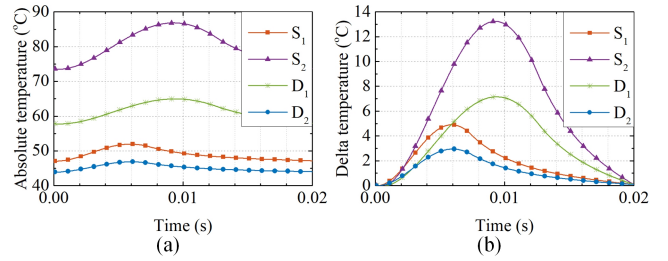
increase in those cases. On the contrary, the loss duration has an inverse impact on D_1, which is illustrated in Figs. 5(c) and (d). Furthermore, since S_2 and D_2 have a similar conduction characteristic in an SM of the MMC, the parameter sensitivity of S_2 and D_2 can be obtained correspondingly.

As illustrated in Fig. 6, the thermal profiles at 50 Hz based on the equivalent loss curves are in close agreement with the thermal profiles obtained from the instantaneous losses with various parameters. The maximum error is approximately 2 °C. Therefore, the proposed equivalent loss curve is effective for simple loading translation at 50 Hz.

Actually, the thermal behaviors at the fundamental frequency of 1 Hz or lower are interesting in the case of variable frequency applications (e.g., motor drive systems). Hence, it is necessary to explore the sensitivity under low frequencies. As shown in Fig. 7, the thermal profiles of S_1 and D_1 at 1 Hz are calculated with different parameters. The thermal profiles obtained from the proposed equivalent loss curve match well with the results based on the original instantaneous losses. It should be noted that a large thermal peak exists at low fundamental frequencies. For instance, the temperature swing
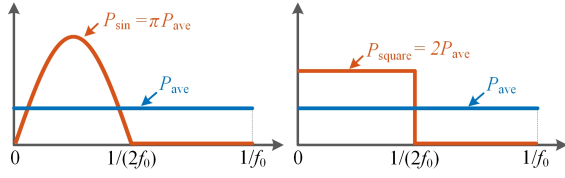
Fig. 10. Fixed half sine loss profile and the fixed square loss profile for junction temperatures swings estimation.
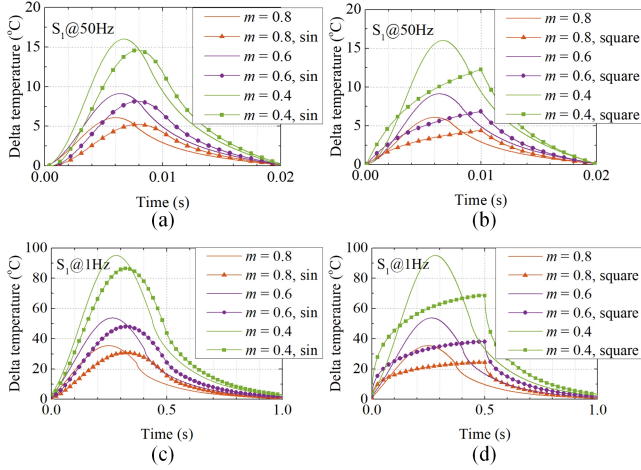

Fig. 12. Output characteristic of the IGBT and the forward characteristic of the diode in different temperatures: (a) IGBT and (b) diode.

Fig. 11. Thermal profiles of S_1 based on the fixed half sine loss profile and the fixed square loss profile with $\varphi = 0°$: (a) 50-Hz fixed half sine loss profile, (b) 50-Hz fixed square loss profile, (c) 1-Hz fixed half sine loss profile, and (d) 1-Hz fixed square loss profile.

Fig. 13. Switching losses of the IGBT. (a) turn-on loss E_{on} and (b) turn-off loss E_{off}.
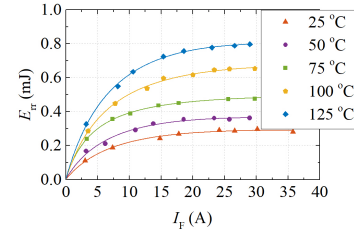
Fig. 14. Recovery loss E_{rr} of the freewheeling diode.

of S_1 is up to 95 °C when $m = 0.4$. Thus, the conventional average models without considering the thermal peaks may not be able to identify potential catastrophic over-temperature failures when the converters operate at low frequencies.

B. Simulation Verification

In order to further validate the effectiveness of the proposed thermal behavior estimation method, an MMC simulation model is built up. The parameters are the same as shown in Table II. The case temperature of the four power devices in an SM is kept at 40 °C in simulations. It should be noted that the loss calculation is out of the scope of this paper, and the average losses for the simulation model are the same as those provided for the temperature estimation. The simulation results are shown in Fig. 8. With the same parameters, the thermal behaviors based on the equivalent loss curve are shown in Fig. 9. Observations from Fig. 8 and 9 demonstrate that the proposed method can predict the thermal behaviors with high accuracy.

C. Comparison with Other Algorithms

Compared to the proposed equivalent loss curve, two prior-art loss profiles (the fixed half sine loss profile and the fixed square loss profile) are also widely accepted [18], [19], [24]. As shown in Fig. 10, although both can meet the same energy condition, the loss duration is fixed to $1/(2f_0)$. Based on the
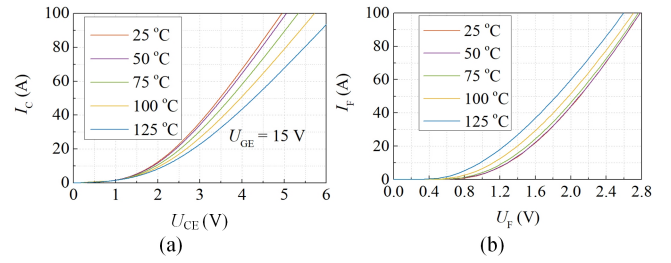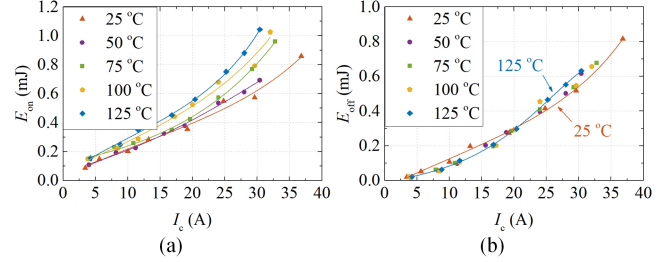
two methods, the dc-bias of the arm currents and the operational parameters of the MMC are neglected, which may lead to inaccuracy. This can be observed from the benchmarking results in Fig. 11.

As seen, with the fixed square wave, the difference is the largest, where the maximum difference is approximately 25 °C at 1 Hz (see Fig. 11(d)). As for the fixed half sine wave shown in Fig. 11(a) and Fig. 11(c), the difference is smaller compared with the results of the square wave, but the maximum difference is still above 10 °C. Note that the fixed half sine loss profile has the same computational complexity compared with the proposed method. However, the difference based on the fixed half sine loss profile is nearly the double of the results based on the proposed method under the same conditions (see Figs. 6 and 7). It is illustrated that, although both the fixed half sine wave and the fixed square wave meet the same energy condition, the power loss distribution during a cycle is also significant for the thermal estimation. Therefore, the fixed square wave and the fixed half sine wave are not sufficient in the estimation of the thermal behaviors at periodic power loss profiles of MMCs.
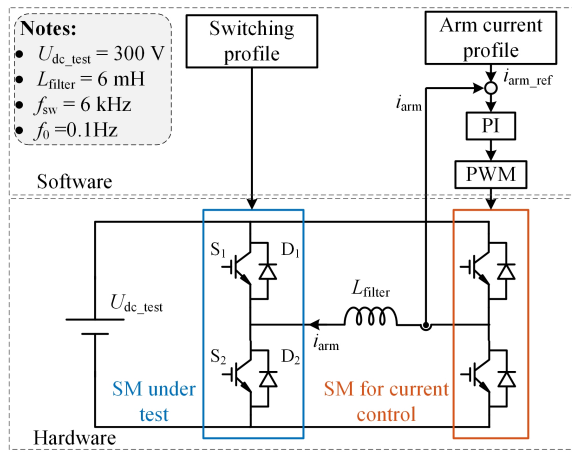
Fig. 15. Experimental platform to evaluate the performance of an SM in the MMC (PI – Proportional Integral control; PWM – Pulse Width Modulation; U_{dc_test} is the dc voltage of power supply; L_{filter} is the filter inductor).
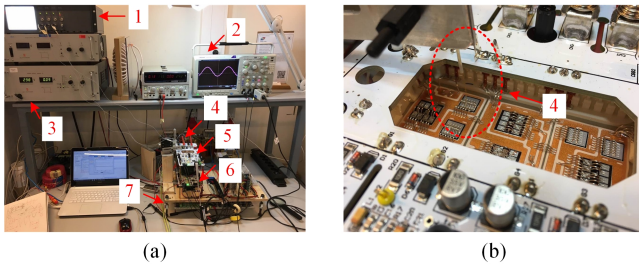

Fig. 16. Experimental platform for the thermal-behavior evaluation of an SM in MMCs: (a) photo of the set-up and (b) zoom-in view of the IGBT module with optical fibers for temperature measurement. (1: fiber optical signal conditioner, 2: oscilloscope, 3: dc power supply, 4: thermal optical fiber, 5: SM under test, 6: SM for control, and 7: controller.)

V. IGBT CHARACTERIZATION AND EXPERIMENTAL RESULTS

In order to validate the estimation model, experiments have been performed by two steps. The power semiconductors used in this paper are characterized first to obtain the accurate loss information under different temperatures. Then, an experimental platform is built up to test the thermal behaviors at periodic power loss profiles. The test results are also compared with the estimated from the proposed method.

A. Characterization of the IGBT Module

An accurate thermal estimation is dependent on the accurate loss information. However, in many cases, the data-sheet of power devices does not provide loss information under various temperatures or blocking-voltage conditions. Therefore, the characterization of the IGBT module should be performed first to obtain the loss information. An IGBT module from Infineon F4-50R12KS4 (1200 V/50 A) is selected as the power device in the experiments, and its characteristics are obtained by following conduction losses and switching losses.

According to (5) to (7), the conduction losses rely on the output characteristics of IGBTs and diodes. These characteristics are tested in the laboratory using an Agilent B1506A curve

tracer and the temperature is controlled by a Thermostream ATS-515. The test results are shown in Fig. 12.

Switching losses are measured with a double-pulse circuit [18], [25], and the measurement method follows the IEC 60747-9 [26]. The device under test is placed on a hot plate to control the operational temperature, and the blocking-voltage is set as 300 V. The measured switching losses of the IGBT and the diode are illustrated in Figs. 13 and 14. The turn-on losses of the IGBT and the recovery losses of the diode decrease when the temperature decreases; while the turn-off losses of the IGBT are almost constant under various temperatures, as shown in Fig. 13(b). Based on the above characteristics of the power semiconductor devices, more accurate power losses are established, enabling more accurate thermal behavior prediction.

B. Experimental Results

In order to validate the effectiveness of the proposed method, experiments are carried out referring to Figs. 15 and 16. The experimental setup is similar to that in [27], where its effectiveness has been validated. As shown in Fig. 15, the configuration consists of two HB-SMs, where one SM is utilized to emulate the arm current reference and the other SM is fed into a switching profile. The junction temperatures of the power devices are then measured and recorded using Opsens[TM] optical fibers. Noted that the frequency of the periodic power loss profile is set to 0.1 Hz in the experiments since the temperature-probe has a limited transient response. Then, three test conditions are considered:

1) $m = 0.8$, $\varphi = 0°$. Figs. 17(a) and (b) show the thermal profiles of S_1 and D_1, respectively, where $i_{arm} = 7.13 + 17.85\sin(2\pi f_0 t)$ A. The measured peak temperature of S_1 is about 45 °C, and both the simulated and estimated values are about 45.5 °C. The diode D_1 also exhibits similar performances, where the maximum difference between the estimated and the experimental result is less than 1 °C. Note that although the waveform of D_1 is slightly different from the estimated, only the amplitudes are considered in typical reliability issues. Therefore, the proposed temperature estimation method can provide a relatively accurate prediction of the temperature swings.

2) $m = 0.6$, $\varphi = 0°$. When the modulation index decreases to 0.6 with $i_{arm} = 7.13 + 23.78\sin(2\pi f_0 t)$ A, the results are shown in Figs. 17(c) and (d). The maximum temperature of S_1 is roughly 54 °C in the experiment, but the estimated is about 52 °C. The difference between the experiment and the estimated temperature is also around 2 °C for the D_1. This is mainly due to: 1) The absolutely accurate losses are impossible. Even though the adopted IGBT modules have been characterized experimentally under different temperatures, the estimated losses are still a little different from the real losses. 2) The thermal coupling between the chips, and the thermal variations on the thermal grease and the heatsink also have an impact on the measurements. Therefore, if the simulation results are benchmarked, the difference will be smaller than 2 °C.

3) $m = 0.8$, $\varphi = 30°$. When $i_{arm} = 7.13 + 20.59\sin(2\pi f_0 t - 30°)$ A, the thermal profiles are illustrated
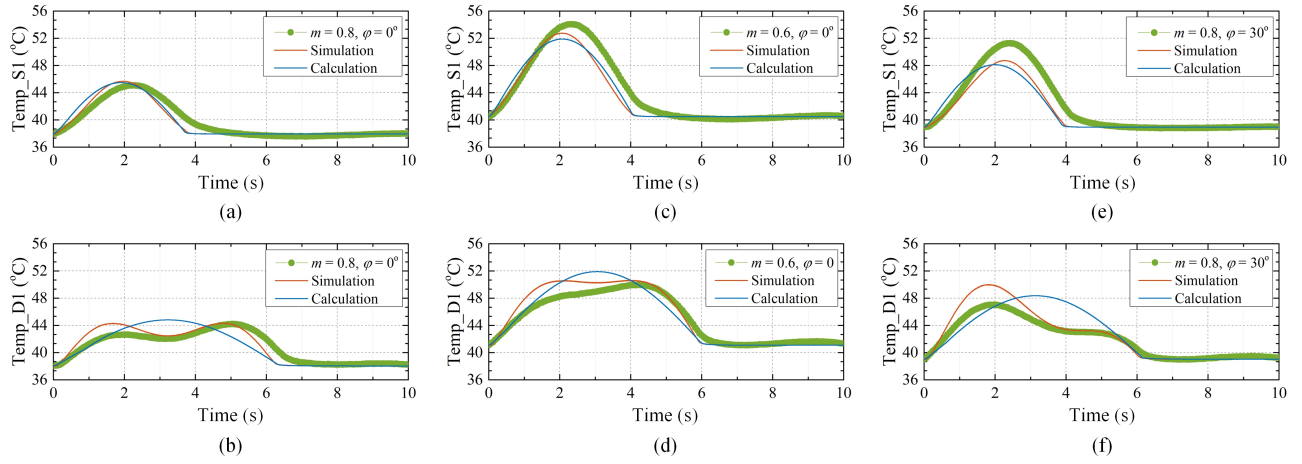
Fig. 17. Junction temperature profile of an IGBT module in an SM: (a) S_1 and (b) D_1 when $m = 0.8$ and $\varphi = 0°$, (c) S_1 and (d) D_1 when $m = 0.6$ and $\varphi = 0°$, and (e) S_1 and (f) D_1 when $m = 0.8$ and $\varphi = 30°$.

in Figs. 17(e) and (f). In this case, the maximum temperature of S_1 is about 51 °C, while the estimated result is only 48 °C. Compared to the simulation result (roughly 49 °C), the difference is smaller. The relatively larger difference compared with the measured value reveals that when the junction temperature has large variations, the negative impact from thermal coupling becomes more significant. For the diode D_1, a similar result is observed, where the maximum difference is smaller than 2 °C.

In addition, it should be noted that the thermal profiles of the diode D_1 have distortions in the experiments and simulations as shown in Figs. 17(b), (d) and (f). This is due to the negative-temperature coefficient of the diode. Referring to the experimental characteristic of the diode in Fig. 12(b), the forward voltage of the diode U_F is reduced when the temperature increases. It means that the power losses of the diode decrease with the temperature rising. However, the temperature swing (i.e., ΔT_j) is the dominant parameter for the lifetime prediction of IGBT modules rather than the thermal waveform [12]. Moreover, the mission-profiled-based lifetime prediction usually needs to process one-year data or more, which means it needs to deal with approximately 1.6×10^9 periodic loss profiles if $f_0 = 50$ Hz. Thus, it is necessary to simplify the profiles to obtain results in the reasonable time. As the result, the negative-temperature coefficient is not considered in the proposed method, while the prediction accuracy is maintained.

In order to further compare the temperature swings, the results are summarized in Table III. Obviously, the results based on the proposed method can achieve an acceptable estimation accuracy compared the time-domain simulation. In contrast, the prior-art methods (i.e., the fixed square wave and the fixed half sine wave) have differences up to about 60%. It should be noted that all the explored methods have the same energy during the cycle of the fundamental frequency. However, larger estimated differences reveal that the power loss distribution during the cycle of the fundamental frequency is also vital for the thermal behavior estimation. In the state-of-the-art methods, it is assumed that the loss conduction time is fixed at a half of the cycle period, which is the reason why

TABLE III
ESTIMATED TEMPERATURE SWINGS BASED ON EXPERIMENTS, SIMULATIONS, THE PROPOSED METHOD, AND THE PRIOR-ART METHODS

Test Conditions		Delta temperatures (°C)				
		Exp*	Simu*	Proposed method	Prior-art methods	
					Square wave	Half sine wave
$m = 0.8,$ $\varphi = 0°$	S_1	7.13	7.73	7.54	3.40	5.34
	D_1	6.15	6.24	6.76	5.77	9.02
$m = 0.6,$ $\varphi = 0°$	S_1	13.58	12.24	11.39	5.73	8.98
	D_1	8.86	9.51	10.82	8.67	13.55
$m = 0.8,$ $\varphi = 30°$	S_1	12.34	9.78	9.18	4.40	6.90
	D_1	7.99	10.97	9.35	7.09	11.07

*Exp – experimental results, Simu – simulated results.

those methods fail to accurately predict thermal-behaviors in MMCs.

Therefore, considering the errors from the loss calculation and thermal coupling in the power devices, the proposed estimated method can provide a relatively accurate prediction of the thermal behaviors under various conditions. The maximum differences between the simulation and the calculation are less than 2 °C, and the maximum differences between the experiment and the calculation are smaller than 3 °C. Thus, the estimated thermal behaviors enable a more accurate lifetime prediction of the IGBT modules, and also enable a better DfR of the entire MMC system.

VI. CONCLUSION

This paper has been investigated the thermal-stress distribution at the periodic power loss profile due to the fundamental-frequency current in the power semiconductor devices of MMC systems. Since a large number of fundamental-frequency thermal stresses accelerate the aging, and it is also essential for cooling systems design, an equivalent loss curve has been proposed to better estimate the thermal behaviors at the fundamental frequency. In this case, the operational parameters of the MMC are also considered. The parameter sensitivity of the proposed method is discussed with a 30-MW MMC model.

Experiments are provided, which validated the effectiveness of the proposed method. Based on the quantitative discussion in this paper, the following conclusions are drawn:

1) Due to the inherent dc-bias arm current of the MMC, thermal behaviors of the power devices are closely coupled with operational parameters;

2) Operational parameters (i.e., m, φ, f_0) are thus considered in the proposed method. Both the loss curves and the estimated thermal behaviors agree well with the results based on original instantaneous power losses;

3) Neither the conventional fixed half sine loss profile nor the fixed square loss profile is sufficient in the estimation of the thermal behaviors at the fundamental frequency for the MMC, since both ignore the impact of operation parameters on its inherent thermal unbalance.

REFERENCES

[1] A. Lesnicar and R. Marquardt, "An innovative modular multilevel converter topology suitable for a wide power range," in *Proc. of IEEE Bologna Power Tech. Conf.*, vol. 3, pp. 1–6, Jun. 2003.

[2] S. Debnath, J. Qin, B. Bahrani, M. Saeedifard, and P. Barbosa, "Operation, control, and applications of the modular multilevel converter: a review," *IEEE Trans. Power Electron.*, vol. 30, no. 1, pp. 37–53, Jan. 2015.

[3] S. Kouro, M. Malinowski, K. Gopakumar, J. Pou, L. G. Franquelo, B. Wu, J. Rodriguez, M. A. Perez, and J. I. Leon, "Recent advances and industrial applications of multilevel converters," *IEEE Trans. Ind. Electron.*, vol. 57, no. 8, pp. 2553–2580, Aug. 2010.

[4] J. J. Jung, H. J. Lee, and S. K. Sul, "Control strategy for improved dynamic performance of variable-speed drives with modular multilevel converter," *IEEE J. Emerg. Sel. Topics Power Electron.*, vol. 3, no. 2, pp. 371–380, Jun. 2015.

[5] M. A. Perez, S. Bernet, J. Rodriguez, S. Kouro, and R. Lizana, "Circuit topologies, modelling, control schemes and applications of modular multilevel converters," *IEEE Trans. Power Electron.*, vol. 30, no. 1, pp. 4–17, Mar. 2015.

[6] M. Hagiwara and H. Akagi, "Control and experiment of pulsewidth-modulated modular multilevel converters," *IEEE Trans. Power Electron.*, vol. 24, no. 7, pp. 1737–1746, Jul. 2009.

[7] K. Ilves, A. Antonopoulos, S. Norrga, and H. P. Nee, "Steady-state analysis of interaction between harmonic components of arm and line quantities of modular multilevel converters," *IEEE Trans. Power Electron.*, vol. 27, no. 1, pp. 57–68, Jan. 2012.

[8] B. Li, R. Yang, D. Xu, G. Wang, W. Wang, and D. Xu, "Analysis of the phase-shifted carrier modulation for modular multilevel converters," *IEEE Trans. Power Electron.*, vol. 30, no. 1, pp. 297–310, Jan. 2015.

[9] Q. Tu, Z. Xu, and L. Xu, "Reduced switching-frequency modulation and circulating current suppression for modular multilevel converters," *IEEE Trans. Power Del.*, vol. 26, no. 3, pp. 2009–2017, Jul. 2011.

[10] G. Konstantinou, J. Pou, S. Ceballos, and V. G. Agelidis, "Active redundant submodule configuration in modular multilevel converters," *IEEE Trans. Power Del.*, vol. 28, no. 4, pp. 2333–2341, Oct. 2013.

[11] O. Cwikowski, H. R. Wickramasinghe, G. Konstantinou, J. Pou, M. Barnes, and R. Shuttleworth, "Modular multilevel converter DC fault protection," *IEEE Trans. Power Del.*, vol. PP, no. 99, pp. 1–1, 2017.

[12] H. Wang, K. Ma, and F. Blaabjerg, "Design for reliability of power electronic systems," in *Proc. IECON 38th Annual Conf. IEEE Ind. Electron. Society*, pp. 33–44, 2012.

[13] S. Yang, A. Bryant, P. Mawby, D. Xiang, L. Ran, and P. Tavner, "An industry-based survey of reliability in power electronic converters," *IEEE Trans. Ind. Appl.*, vol. 47, no. 3, pp. 1441–1451, Mar. 2011.

[14] P. D. Reigosa, H. Wang, Y. Yang, and F. Blaabjerg, "Prediction of bond wire fatigue of IGBTs in a PV inverter under a long-term operation," *IEEE Trans. Power Electron.*, vol. 31, no. 10, pp. 7171–7182, Dec. 2016.

[15] K. Ma, M. Liserre, F. Blaabjerg, and T. Kerekes, "Thermal loading and lifetime estimation for power device considering mission profiles in wind power converter," *IEEE Trans. Power Electron.*, vol. 30, no. 2, pp. 590–602, Mar. 2015.

[16] W. Lai, M. Chen, L. Ran, O. Alatise, S. Xu, and P. Mawby, "Low ΔT_j stress cycle effect in IGBT power module die-attach lifetime modeling," *IEEE Trans. Power Electron.*, vol. 31, no. 9, pp. 6575–6585, Nov. 2016.

[17] H. Liu, K. Ma, Z. Qin, P. C. Loh, and F. Blaabjerg, "Lifetime estimation of MMC for offshore wind power HVDC application," *IEEE J. Emerg. Sel. Topics Power Electron.*, vol. 4, no. 2, pp. 504–511, Sep. 2016.

[18] A. Wintrich, N. Ulrich, T. Werner, and T. Reimann, *Application Manual Power Semiconductors.* Nuremberg, Germany: Semikron Int.GmbH, 2015.

[19] "Dimensioning program IPOSIM for loss and thermal calculation of Infineon IGBT modules," Tech. Rep.

[20] H. Akagi, "Classification, terminology, and application of the modular multilevel cascade converter (MMCC)," *IEEE Trans. Power Electron.*, vol. 26, no. 11, pp. 3119–3130, Nov. 2011.

[21] K. Ma, M. Liserre, and F. Blaabjerg, "Operating and loading conditions of a three-level neutral-point-clamped wind power converter under various grid faults," *IEEE Trans. Ind. Appl.*, vol. 50, no. 1, pp. 520–529, Jun. 2014.

[22] N. C. Sintamarean, F. Blaabjerg, H. Wang, F. Iannuzzo, and P. De Place Rimmen, "Reliability oriented design tool for the new generation of grid connected PV-inverters," *IEEE Trans. Power Electron.*, vol. 30, no. 5, pp. 2635–2644, May. 2015.

[23] K. Sharifabadi, L. Harnefors, H.-P. Nee, R. Teodorescu, and S. Norrga, *Design, Control and Application of Modular Multilevel Converters for HVDC Transmission Systems.* John Wiley & Sons, 2016.

[24] L. Pan and C. Zhang, "A high power density integrated charger for electric vehicles with active ripple compensation," *Math. Probl. Eng.*, 2015.

[25] U. Nicolai and A. Wintrich, "Determining switching losses of SEMIKRON IGBT Modules," Tech. Rep., 2014.

[26] IEC-60749-34, "Semiconductor devices-Discrete devices-Part 9: Insulated-gate bipolar transistors (IGBTs)," Tech. Rep., 2007.

[27] F. Hahn, M. Andresen, G. Buticchi, and M. Liserre, "Thermal analysis and balancing for modular multilevel converters in HVDC applications," *IEEE Trans. Power Electron.*, pp. 1–10, 2017.
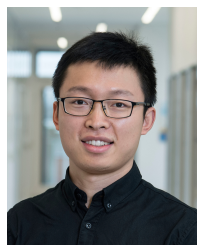
Yi Zhang (S'17) was born in Sichuan, China. He received the B.S. and M.S. degrees in electrical engineering from Harbin Institute of Technology, Harbin, China, in 2014 and 2016, respectively. He is currently working toward the Ph.D. degree with the Center of Reliable Power Electronics (CORPE), Aalborg University, Aalborg, Denmark. He was a visiting scholar with Center for Advanced Power Technology, National Tsinghua University, Taiwan, from June to August 2013.

His current research interests include the reliability of power electronics including the Physics-of-Failure (PoF) analysis of reliability critical components and Design for Reliability (DfR) methods for power electronic applications, high-power electronics, and multilevel converters.

Huai Wang (M'12-SM'17) received the B.E. degree in electrical engineering, from Huazhong University of Science and Technology, Wuhan, China, in 2007 and the Ph.D. degree in power electronics, from the City University of Hong Kong, Hong Kong, in 2012.

He is currently an Associate Professor and a Research Thrust Leader in the Center of Reliable Power Electronics (CORPE), Aalborg University, Aalborg, Denmark. He was a Visiting Scientist with the ETH Zurich, Switzerland, from Aug. to Sep. 2014, and with the Massachusetts Institute of Technology (MIT), USA, from Sep. to Nov. 2013. He was with the ABB Corporate Research Center, Switzerland, in 2009. His research addresses the fundamental challenges in modelling and validation of power electronic component failure mechanisms, and application issues in system-level predictability, condition monitoring, circuit architecture, and robustness design. He has contributed a few concept papers in the area of power electronics reliability, filed four patents on capacitive DC-link inventions, and co-edited a book.

Dr. Wang received the Richard M. Bass Outstanding Young Power Electronics Engineer Award from the IEEE Power Electronics Society in 2016, and the Green Talents Award from the German Federal Ministry of Education and Research in 2014. He is currently the Award Chair of the Technical Committee of the High Performance and Emerging Technologies, IEEE Power Electronics Society. He serves as an Associate Editor of IET POWER ELECTRONICS, IEEE JOURNAL OF EMERGING AND SELECTED TOPICS IN POWER ELECTRONICS, and IEEE TRANSACTIONS ON POWER ELECTRONICS.
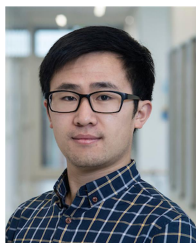
Zhongxu Wang (S'17) received the bachelor's and master's degrees in electrical engineering from Harbin Institute of Technology, Harbin, China in 2014 and 2016, respectively. He is currently working towards his Ph.D. degree in Aalborg University, Aalborg, Denmark.

His research interests include adaptive thermal control and condition monitoring of modular multilevel converters and reliability in power electronics.

Yongheng Yang (S'11-M'15-SM'17) received the B.Eng. degree in electrical engineering and automation from Northwestern Polytechnical University, Shaanxi, China, in 2009 and the Ph.D. degree in electrical engineering from Aalborg University, Aalborg, Denmark, in 2014.

He was a postgraduate student at Southeast University, China, from 2009 to 2011. In 2013, he was a Visiting Scholar at Texas A&M University, USA. Dr. Yang has been with the Department of Energy Technology, Aalborg University since 2014, first as a Postdoc researcher, then an Assistant Professor, and now an Associate Professor. He has been focusing on grid integration of renewable energies, power electronic converter design, analysis and control, and reliability in power electronics.

Dr. Yang served as a Guest Associate Editor of IEEE Journal of Emerging and Selected Topics in Power Electronics and a Guest Editor of Applied Sciences. He is an Associate Editor of CPSS Transactions on Power Electronics and Applications.

Frede Blaabjerg (S'86-M'88-SM'97-F'03) was with ABB-Scandia, Randers, Denmark, from 1987 to 1988. From 1988 to 1992, he was a Ph.D. Student at Aalborg University, Aalborg, Denmark and received the PhD in Electrical Engineering in 1995. He became an Assistant Professor in 1992, Associate Professor in 1996, and Full Professor of power electronics and drives in 1998 at the same place. His current research interests include power electronics and its applications such as in wind turbines, PV systems, reliability engineering, power quality and adjustable speed drives.

He has received 18 IEEE Prize Paper Awards, the IEEE PELS Distinguished Service Award in 2009, the EPE-PEMC Council Award in 2010, the IEEE William E. Newell Power Electronics Award 2014 as well as the Villum Kann Rasmussen Research Award 2014. He was an Editor-in-Chief of the IEEE TRANSACTIONS ON POWER ELECTRONICS from 2006 to 2012. He is nominated in 2014, 2015 and 2016 by Thomson Reuters to be between the most 250 cited researchers in Engineering in the world. In 2017 he became Doctor Honoris Causa at University of Politehnica in Timisoara, Romania.